Reassessment of hydrate destabilization mechanisms offshore west Svalbard confirms link to recent ocean warming

Akash Trivedi[1*], Sudipta Sarkar[1], Hector Marin-Moreno[2], Timothy A. Minshull[3], Pippa L. Whitehouse[4], Utpal Singh[1]

Affiliations:

[1]Department of Earth and Climate Science, Indian Institute of Science Education and Research Pune, Pune, 411008, India

[2]Norwegian Geotechnical Institute, PB 3930 Ullevål Stadion, NO-08906 Oslo, Norway

[3]School of Ocean and Earth Science, University of Southampton, Waterfront Campus, European Way, Southampton SO14 3ZH, UK

[4]Department of Geography, Durham University, Durham, DH1 3LE, UK

*Correspondence to: Akash Trivedi (trivedi.akash@students.iiserpune.ac.in)

Key Points:

- We examine the effect of the past 11000 years' bottom water temperature and relative sea level change on Arctic gas hydrate dynamics.
- Relative sea-level fall over the past 8 ka thins the hydrate layer, but several bottom water warming pulses also contribute to its dissociation.
- Simulation confirms present-day gas seeps and observed chloride anomaly can be explained by thermal dissociation of hydrate over 1978-2016.

Abstract

The stability of methane hydrates at the feather edge of hydrate stability on the upper continental slope (UCS) is prone to ocean warming and relative sea-level (RSL) change. West of Svalbard, methane seeps on the UCS were initially proposed to result from hydrate destabilization resulting from four decades of warming of Atlantic bottom water. Alternatively, it has been proposed that hydrate dissociation was triggered by RSL fall due to isostatic rebound over the past 8000 years rather than recent bottom water temperature (BWT) rise. Here we address these two contrasting hypotheses by simulating the impact of 11000 years of BWT and RSL change on hydrates located at the UCS off west Svalbard. Our numerical simulation considers multiphase fluid and heat flow coupled with hydrate formation and dissociation. We used two reconstructions of local ice history (UiT and ICE-6G_C) that predict contrasting results for the local sea-level history. Over the past 8000 years, the UiT model predicts a fall in RSL on the UCS, while the ICE-6G_C model, which provides a better fit to nearby coastal RSL observations, predicts a continuous rise. Our modeling shows that whilst long-term RSL fall would progressively thin the region of hydrate stability, the abrupt rise in BWT enhances hydrate dissociation. Even in the model with an RSL rise, the increase in BWT causes hydrate destabilization and pore water freshening that matches observations. We conclude that recent ocean warming plays a critical role in hydrate dissociation west of Svalbard regardless of the longer term sea-level history.

Plain language summary:

Methane hydrate is an ice-like substance that is stable at the low temperatures and high pressures found in the mud and sand that builds up at the edges of oceans. Hydrate can melt and vent methane gas into the ocean if the ocean warms or sea-level falls. Drilling in a region of such venting west of the Arctic Archipelago of Svalbard in 2016 confirmed that it was caused by the melting of hydrate, but the cause of this melting is debated. Proposed causes are ocean warming during 1978–2016, or relative sea-level fall since 8000 years ago as the ocean floor near Svalbard rose due to the removal of the weight of the melting Svalbard ice sheet. We used a computer model to study the impact of changes in ocean temperature and sea level on this hydrate since 11000 years ago. We found that sea-level fall causes the hydrate to melt, but there are periods of colder ocean temperatures when it can re-form. Sea-level rise stabilizes the hydrate, but ocean warming can override its effect, leading to the hydrate melting that is inferred during 1978–2016. We conclude that ocean warming played a critical role in hydrate melting.

1. Introduction

The effects of ocean warming are clearly visible across the Arctic (Hassol, 2004), as evidenced by the disappearance of sea ice (Comiso et al., 2008; Piechura & Walczowski, 2009) and enhanced glacier melting (Osterkamp, 2005; Nagornov et al., 2006; Anthony et al., 2012). Dissociation of methane hydrates has also been linked with past climate warming (Nisbet, 1990; Dickens, 2003; Kennett et al., 2003), and there is concern about the stability of methane hydrate deposits trapped in Arctic marine sediments (Kretschmer et al., 2015). Hydrate at the feather edge of its stability zone, where the base of this zone outcrops on the upper continental slope, are particularly vulnerable to thermal destabilization. The marine sediments of the Fram Strait, the Arctic-Atlantic gateway located in the western Svalbard region, host widespread methane hydrates (Figure 1a, Sarkar et al., 2012; Dumke et al., 2016; Minshull et al., 2020). A marine geophysical expedition in 2008 discovered plumes of methane bubbles emanating from the seafloor close to and further up-slope of the present-day upper limit of methane hydrate stability on the eastern margin of the Fram Strait (Westbrook et al., 2009). Here warm and saline Atlantic water brings heat into the Arctic Ocean through the Fram Strait via the West Spitsbergen Current. This Atlantic water is inferred to have warmed the bottom water temperature (BWT) from 2º to 3º C over the past four decades, resulting in the migration of the feather edge of methane hydrate stability from 370 m to 410 m depth (Westbrook et al., 2009). Westbrook et al. (2009) proposed that these methane bubble plumes indicate thermal degradation of the hydrates at the landward limit of hydrate stability.

Several subsequent marine surveys consistently found methane seeps (Sahling et al., 2014; Mau et al., 2017; Veloso-Alarcon et al., 2019) between 370 m and 410 m water depths on the upper slope (Figure 1b). The gas flare density and methane release rates are reduced during the winter when the temperatures are substantially lower than in summer (Veloso-Alarcon et al., 2019; Ferré et al., 2020). This suggests that seasonal fluctuations in BWT can lead to repeated episodes of hydrate formation and dissociation (Berndt et al., 2014; Veloso-Alarcon et al., 2019; Ferré et al., 2020). However, the link between methane seepage and anthropogenic ocean warming has been questioned because the presence of seep carbonates in this area suggests that seepage has been active for >8,000 yr (Berndt et al., 2014). Numerical simulation of the response of gas hydrates to BWT changes was previously carried out considering past and future ocean temperature variations (Reagan et al., 2011; Thatcher et al., 2013; Marín-Moreno et al., 2013; Marín-Moreno et al., 2015). Results from these studies indicated that for hydrate shallower than a few metres beneath the seabed, bottom water warming since the late 1970s has produced gas from hydrate dissociation. However, these studies did not account for the effect of relative sea level (RSL) change on hydrate stability.

Hydrate dissociation off west Svalbard was first geochemically confirmed by Wallmann et al. (2018). Pore water samples collected from sediments during a “MeBo” seafloor drilling experiment conducted in 2016 at a water depth of 391 m (Figure 1b) showed a decline in chloride concentration at 15–22 m below the seabed, indicating freshening caused by hydrate dissociation. Based on the University of Tromsø (UiT) RSL model (Patton et al., 2017), Wallmann et al. (2018) inferred that approximately 8000 years ago, the glacial isostatic rebound rate exceeded the rate of eustatic sea-level rise. The resulting RSL fall and consequent drop in hydrostatic pressure led to hydrate destabilization. In their model, hydrate dissociation was completed 1000 years before the present (BP, where ‘Present’ is considered as 2016). Hydrate could re-form in the model during colder BWT conditions in the late1970s (Ferré et al., 2012; Wallmann et al., 2018). Wallmann et al. (2018) concluded that a 1°C linear rise in BWT over 1980–2016 would be insufficient to result in hydrate dissociation. However, in their modeling they did not account for the decadal-scale temperature fluctuations observed in the measured records. Such variations can impact hydrate dynamics and methane flow at the seabed, and therefore, should be included in a realistic assessment of whether recent bottom water warming could have caused the observed hydrate dissociation.

Glacial retreat across Svalbard took place about 13000 years BP (Landvik et al., 2008), causing rapid seafloor uplift and a prominent relative sea-level (RSL) drop over 8–12 ka along the western Svalbard coast (Forman et al., 2004). RSL change at the MeBo drill site is not constrained by data and must be estimated by geodynamic modeling. Comparison of observed and predicted RSL change based on various deglacial scenarios has revealed the inadequacy of some models in reproducing observations of RSL change throughout the Barents Sea region (Auriac et al., 2016). The ICE-6G_C scenario correctly predicts a fall in RSL over 8–12 ka in west Svalbard (Auriac et al., 2016) but, in contrast to the UiT model employed by Wallmann et al. (2018), it predicts RSL rise at the MeBo site during the past 8000 years (see Section 3.3). Ultimately it is not possible to confirm which scenario is correct. Therefore, we consider both the UiT and ICE-6G_C RSL scenarios to examine the role of pressure in hydrate dynamics west of Svalbard.

Here we address the limitations of previous studies and place further constraints on hydrate dissociation processes through coupled heat and mass transfer numerical simulations of the impact of 11000 years of ocean temperature and RSL change on hydrate located at the upper continental slope off west Svalbard. We have attempted to reproduce the present-day chloride anomaly observed in the sediment core collected at 391 m water depth (Wallmann et al., 2018) by varying the initial hydrate saturation and considering realistic RSL and BWT reconstructions, including decadal and seasonal temperature fluctuations. Based on this modeling, we conclude that rising BWT plays a dominant role in hydrate destabilization, potentially overprinting the effect of any ongoing RSL rise or fall.

2. The West Svalbard Margin

The west Svalbard continental margin has experienced repeated Pliocene–Pleistocene glaciations and deglaciations that affected sea level, sedimentation, and erosion patterns (Landvik et al., 2008). Fast-flowing ice streams carved out the Kongsfjorden, Isfjorden, and Bellsund cross-shelf troughs (KT, IT, and BT, Figure 1a). The present-day shelf break represents the maximum extent reached by the ice sheet and grounded ice streams (Solheim et al., 1996; Knies et al., 2009). Our study area (Figure 1b) is located in the inter-fan region between the Kongsfjorden and the Isfjorden cross-shelf troughs (Sarkar et al., 2011). Using multi-channel reflection seismic data, Sarkar et al. (2012) identified a gas hydrate bottom-simulating reflector (BSR) (Figures 1a and 1b) beneath the upper continental slope. The BSR represents the boundary between gas hydrates above and free gas below (Shipley et al., 1979). There is no evidence of a BSR in water depths shallower than ~600 m (Sarkar et al., 2012); instead, there is seismic evidence of gas accumulations (400–700 m water depths), as evidenced by low-velocity pockets and negative-polarity bright spots within the top 75 m sediment column below the seabed (Chabert et al., 2011). In addition, regions of anomalously high electrical resistivity suggest the presence of hydrate within its stability field (Goswami et al., 2016).

The Pliocene–Pleistocene sediments on the shelf and upper continental slope are predominantly glaciogenic in origin. The marine hemipelagic sediments are interbedded with glacial debris flow units at the upper slope (Sarkar et al., 2011, 2012). The MeBo drilling experiment drilled a mixture of hemipelagic sediments and poorly-sorted glacial debris consisting of a broad range of grain sizes, from clay to sand with gravel to pebble-sized clasts in variable amounts (Wallmann et al., 2018). During the deglaciations, meltwater discharge on the upper continental slope resulted in turbidity currents cascading down the slope, depositing sand and silt-rich sediments (Vorren et al., 1998). The lithological heterogeneity strongly influences fluid flow below the methane seepage sites, for example, the flow of gas is impeded by the glaciogenic debris. Lateral fluid migration occurs along the sand and silt-rich permeable sediments, and near-vertical flow occurs through fractures within poorly stratified, low-permeability glaciogenic sediments (Haacke & Westbrook, 2006; Haacke et al., 2009; Sarkar et al., 2012; Thatcher et al., 2013).

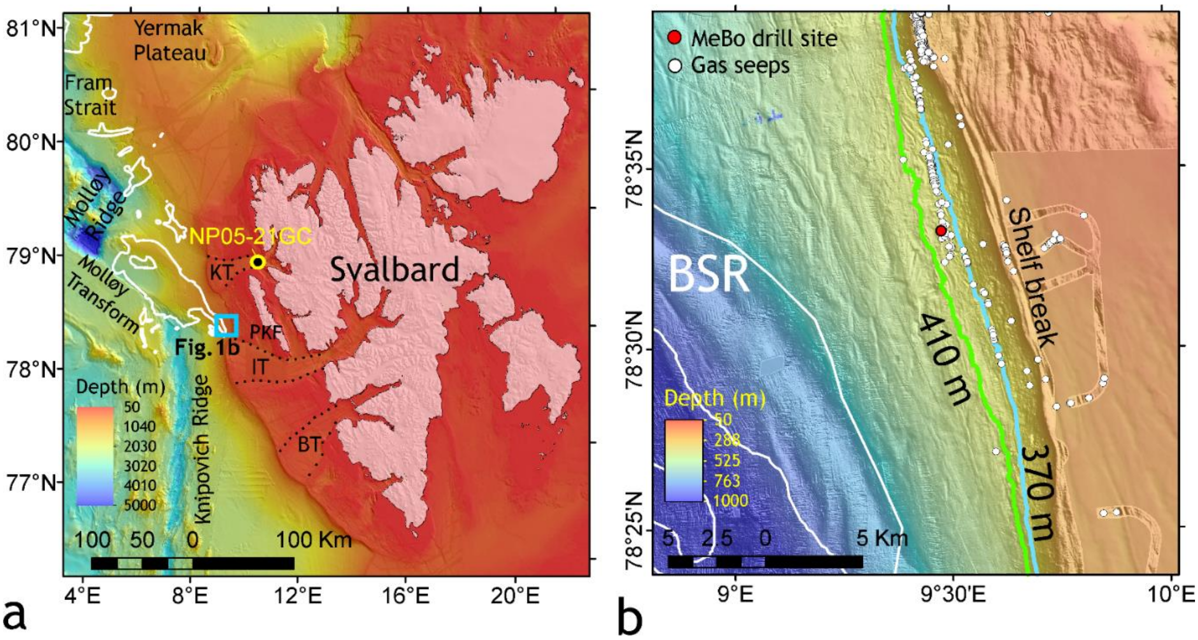

Figure 1. West Svalbard continental margin with bathymetry compiled from various sources, such as Norwegian Hydrographic Survey, swath-bathymetry from JR211 cruise (Sarkar et al., 2012), and International Bathymetric Chart of the Arctic Ocean (Jakobsson et al., 2020). (a) The Kongsfjorden (KT), Isfjorden (IT), and Bellsund (BT) cross-shelf troughs are the palaeo-ice stream pathways dissecting the shelf. The study area is located between the KT and IT and west of Prins Karl Forland (PKF). The solid white line represents the extent of the seismic bottom simulating reflector (BSR) (Sarkar et al., 2012; Dumke et al., 2016). The hydrate province is bounded by the Molløy Transform Fault that links the Knipovich Ridge and the Molløy Ridge. The sediment core NP05-21GC (yellow dot) is located at 327 m water depth on the Kongsfjorden shelf west of Svalbard (Rasmussen et al., 2014). (b) Gas seeps on the upper continental slope are located between 370 and 410 m water depths (Sarkar et al., 2012), which correspond to the theoretical limit of methane hydrate stability at 2°C and 3°C bottom water temperatures respectively. The MeBo drill site is located at 391 m water depth.

3. Data and Method

3.1. Modeling approach

We performed 1D numerical simulations of vertical fluid and heat flow coupled with hydrate formation and dissociation using the TOUGH+Hydrate code v1.5 (Moridis et al., 2014). We used an equilibrium hydrate formation and dissociation model with three mass components, i.e., methane, water, and salt (NaCl), partitioned into four possible phases (gas hydrate, ice, gas, and liquid). The model considers conductive and convective heat transport, pressure-driven transport of water and methane gas (Darcy's flow), advective and diffusive transport of dissolved methane and salt in water, and latent heat of hydrate formation and dissociation.

Model initialization at 11200 yr BP was done assuming a hydrostatic pressure gradient, constant heat flow at the base of the model of 10×10^{-2} W m^{-2} and water saturated sediment thermal conductivity of 2 Wm^{-1}K^{-1} (Riedel et al., 2018), generating a geothermal gradient of 50° C/km, 3.5 wt% pore water salinity and appropriate BWT and pressure in the top cell of the model (Figure 2a). We used the BWT and pressure values from the reconstructed curves discussed in sections 3.2 and 3.3. Model initialization is done based on various BWT and RSL scenarios (Supplementary Figure 1). The model has a constant cell thickness of 0.5 m from 1 mm to a maximum depth of 750 m and assumes a present-day water depth of 391 m. The topmost cell where the top boundary conditions are applied has a thickness of 1 mm and represents the ocean bottom.

The base of the sulfate reduction zone at the MeBo site is 5–7 m (Thatcher et al., 2013; Marín-Moreno et al., 2013; Marín-Moreno et al., 2015 and Wallmann et al., 2018). To represent this, we assume the top 7 m of the sediment column is hydrate-free in the starting model, but we do not consider that this zone was hydrate-free throughout the simulation. The sulfate reduction zone comprises marine anoxic sediments within which there is a decline in sulfate concentration, and dissolved methane is consumed by anaerobic oxidation (Boetius and Wenzhöfer, 2013; Borowski et al., 1996). We have not modeled this process. The Holocene sedimentation rate is negligible, only 4 cm kyr^{-1} (Panieri et al., 2016); therefore, sedimentation is not included in the modeling.

The initial hydrate layer in our model was placed up to the base of methane hydrate stability zone (MHSZ) (Figure 2b). We considered a range of initial hydrate saturations (e.g., 9–60%) for different scenarios. Since no hydrate was recovered during MeBo drilling experiment, this initial hydrate should completely melt. We assume an initial value for gas saturation below the MHSZ of 2–4% based on geophysical evidence of gas in the inter-fan region in a depth range of 480–1285 m on the upper slope (Chabert et al., 2011). Goswami et al. (2016) inferred a much larger gas saturation (>10%) around the landward edge of the GHSZ based on high resistivity. However, the high resistivity values could also be influenced by the presence of authigenic carbonates. We used 2–4% gas below the hydrate stability zone based on earlier models (Marín-Moreno et al., 2013 and Marín-Moreno et al., 2015). The gas was pure methane (James et al., 2011).

We assumed an initial hydrate-free uniform intrinsic (absolute) permeability of 10^{-13} m^2, which is 2–4 orders of magnitude higher than the permeability of hemipelagic glaciomarine sediments (Table S1). We adopted the value from Thatcher et al. (2013), who argued that shallow glacial sediments could rarely sustain a low intrinsic permeability during rapid gas release from hydrate dissociation because the pore pressure will surpass the lithostatic load within a few years of the onset of hydrate dissociation (Thatcher et al., 2013), subsequently leading to the development of fractures that enhance permeability. Hence this high value of intrinsic permeability simulates the effects of fracture permeability. In the scenario they investigated, Thatcher et al. (2013) found that gas appeared at the seabed in response to recent decadal-scale warming, consistent with observations, while if lower permeabilities were used, gas release into the ocean was delayed. In the presence of hydrate in the pore space, there is a reduction in the intrinsic permeability, which is accounted for in the model by using the Evolving Porous Medium model (Moridis et al., 2014; Table S1). The irreducible gas saturation and water saturation are 2 and 12%, respectively, consistent with laboratory measurements (Liu and Flemings, 2007). We note that, to our knowledge, there is no published laboratory data from sediment cores in our study area to better constrain the irreducible gas saturation. We also incorporated multiphase molecular diffusion. Methane flux by molecular diffusion is slow compared to the free gas flow and advection mechanisms, but the simulation time is long; therefore, transport by molecular diffusion can be important.

Changes in BWT and RSL were applied to the model at yearly intervals by changing the temperature and pressure in the top cell. Our model includes the instantaneous response of the sediment column to RSL-induced pressure changes and addresses the process of hydrate dissociation and reformation; for example, the model accounts for the elevated pore-pressure and salinity drop that occur during hydrate dissociation, which can further inhibit melting, as suggested by Liu and Flemings (2009). A summary of the properties used in the models is provided in Table S1.

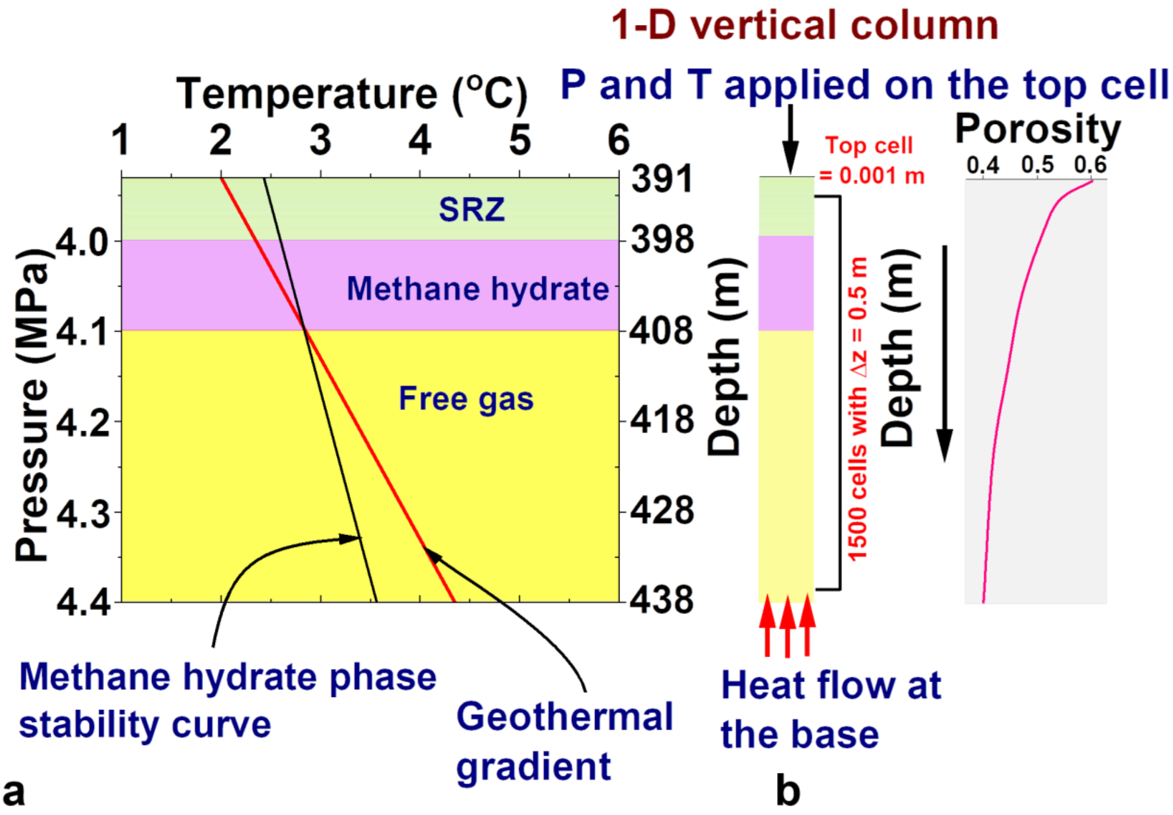

Figure 2. Schematic representation of the model domain at a water depth of 391 m. (a) Methane hydrate stability shown on the Temperature vs. Pressure (Depth) plot. The thickness of the methane hydrate stability is calculated using the geothermal gradient (red line) and the methane hydrate phase stability curve (black line). SRZ denotes the sulfate reduction zone (green area). Methane hydrate-bearing sediments are represented by the purple, and the free gas zone by the yellow colour. (b) Schematic representation of a 1-D vertical sediment column with the boundary conditions. Time-dependent pressure and temperature values are applied as boundary conditions on the top cell while a constant heat source is maintained at the bottom cell. The porosity depth profile is shown by the pink curve.

3.2. Sea bed temperature history

Rasmussen et al. (2014) reconstructed the BWT west of Svalbard over the past 11200 years based on two proxies – (1) benthic foraminiferal census counts (BWT_{TF}) and (2) benthic foraminifera $\delta_{18}O$ values (BWT_{C}) from the sediment core NP05-21GC taken at 327 m water depth on the Kongsfjorden shelf west of Svalbard. NP05-21GC is closest sediment core to the methane seepage site on the upper continental slope (Figure 1a). It is currently bathed by warm Atlantic water (Sarkar et al., 2015), and hence we assume that the reconstructed BWT values well represent past temperature variations of the Atlantic water mass.

The BWT_{C} temperatures, based on $\delta_{18}O$ values in *Cibicides lobatulus*, are influenced by summer conditions since it calcifies during the summer. Temperatures derived using this approach may therefore be biased warm. The BWT_{C} curve shows incursions of warmer

Atlantic water during the early Holocene (11500–6000 years BP) and a subsequent temperature dip during 5000–2000 years BP (Figure 3a). BWT_{TF} (also shown in Figure 3a) shows a smoother curve compared to BWT_C because its reconstruction relies on annual faunal counts (Rasmussen et al., 2014). Since we do not know which is the most representative temperature curve, we considered both the temperature series.

In addition, Marín-Moreno et al. (2013) compiled measured and estimated temperature records at 400 m water depth on the West Svalbard continental margin for the past two millennia. For the years A.D. 1–1900, they used 50-year-running summer temperature means at 50 m water depth, derived from planktic foraminifera proxy (Spielhagen et al., 2011), and applied appropriate scaling to predict the temperature at 400 m depth based on the ocean/sea-ice model NEMO at 1/12° resolution (ORCA12) (Madec, 2012). We use the resulting BWT_M curve of Marín-Moreno et al. (2013) (Figure 3b) in a specific modeling scenario (refer to section 4.3).

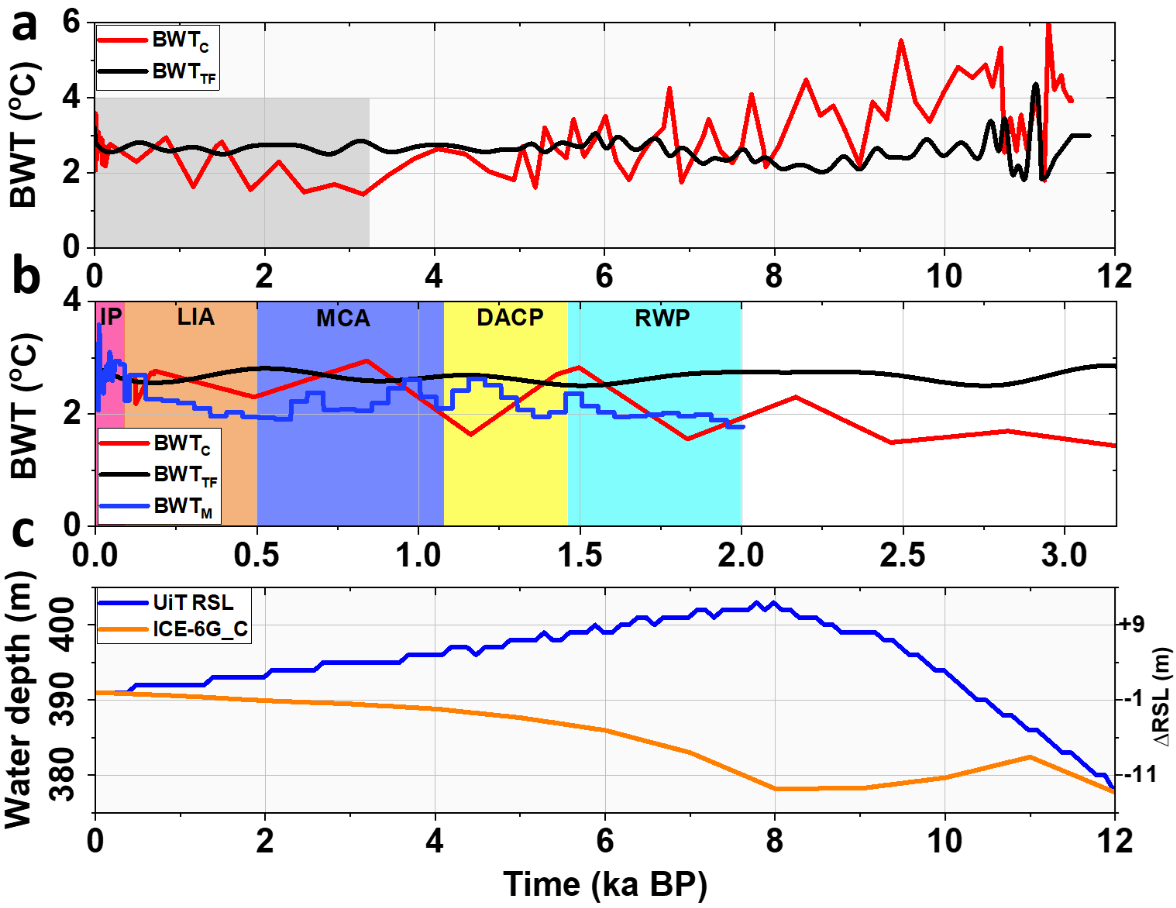

Figure 3. BWT and RSL changes used as model boundary conditions. (a) Bottom water temperatures derived from shelf core NP05-21GC (327 m depth) based on a benthic foraminifera transfer function (BWT_{TF}) and oxygen isotopes (BWT_C) (Rasmussen et al., 2014) for the period 11.7–0 ka. (b) Reconstructed BWT_M values from Marín-Moreno et al. (2013) during the Roman Warm Period (RWP, 2005–1405 BP), the Dark Ages Cold Period (DACP, 1405–1105 BP), the Medieval Climate Anomaly (MCA, 1105–505 BP), the Little Ice Age (LIA, 505–100 years BP), and the Industrial period (IP, 100–present) (Spielhagen et al., 2011). For the IP, BWT values are from Polyakov (2004) for 1900-1950, Holliday et al. (2008) for 1950–1975, and CTD-based near-seabed temperature values from Westbrook et al.

(2009) and Thatcher et al. (2013) for 1975–2005. (c) Modeled RSL (relative to present) over the past 12000 years at the MeBo site (Fig. 1b) based on the University of Tromsø (UiT) ice load history and Earth rheology model (Auriac et al., 2016) (UiT RSL) and the ICE-6G_C scenario (ICE-6G_C RSL).

3.3. Relative sea-level change

We considered two relative sea-level (RSL) change scenarios during the past 11200 years (Figure 3c) – (1) the RSL values of Wallmann et al. (2018), which are based on the University of Tromsø (UiT) model of Eurasian ice sheet change (Patton et al., 2017), and (2) the RSL change predicted using the global ICE-6G_C ice history model (Peltier et al., 2015; Auriac et al., 2016). The UiT model of ice sheet change was developed using a thermo-mechanical ice model coupled to a climate model (Patton et al., 2017). The UiT RSL curve used here is an extended version of the curve used by Wallmann et al. (2018), which only extended back to 8 ka BP. It was derived by combining the isostatic response to ice load change, calculated using an elastic lithosphere/relaxed asthenosphere model (Le Meur and Huybrechts, 1996), with a eustatic sea-level curve (Waelbroeck et al. 2002).

The ICE-6G_C model is the updated version of its predecessor ICE-5G (Argus et al., 2014; Peltier et al., 2015). ICE-6G_C was tuned and tested using a suite of relative sea-level data, GPS observations of vertical motion, and time-dependent gravity change. Auriac et al. (2016) found that ICE-6G_C provides the best fit to RSL data across the Barents Sea when combined with an Earth model that has a relatively thin lithosphere (71 km), an upper mantle viscosity of 0.2×10^{21} Pa s, and a lower mantle viscosity of 2×10^{21} Pa s. However, when seeking to fit RSL data from Svalbard alone they identified an optimum Earth model with 96 km lithosphere, 0.3×10^{21} Pa s upper mantle viscosity, and 2×10^{21} Pa s lower mantle viscosity (Auriac et al., 2016; their Table 4). We combined the ICE-6G_C ice history with two lithosphere thickness values, 71 and 96 km, and a range of combinations of upper and lower mantle viscosities (Supplementary Figure 2). A global glacial isostatic adjustment (GIA) model was used to predict gravitationally self-consistent RSL for the ICE-6G_C model at Prins Karl Forland – to compare with existing RSL data from Forman et al. (2004) – and the MeBo site (Supplementary Figure 2 and Table S2). Differences between model predictions are small (<5 m) during the period of interest, and we use the model characterized by 71 km lithosphere thickness, 0.2×10^{21} Pa s upper mantle viscosity, and 5×10^{21} Pa s lower mantle viscosity.

We use both the UiT and the ICE-6G_C ice history models to provide RSL boundary conditions when modeling the past behaviour of methane hydrates because they predict contrasting behaviour over the past 11000 years (Figure 3c). The UiT scenario predicts a rise in RSL (increase in water depth) for the upper slope site over 11200–8000 years BP followed by a fall. The ICE-6G_C model predicts steady RSL prior to 8000 years BP and a steep RSL rise between 8000–4000 years BP, followed by a gentler rise during the last 4000 years.

4. Results

We ran the 1-D hydrate model with four different plausible combinations of BWT and RSL changes, viz. BWT_{TF} & UiT RSL, BWT_{TF} & ICE-6G_C RSL, BWT_C & UiT RSL, BWT_C & ICE-6G_C RSL (Figures 3a and 3c) to understand the past behavior of methane hydrates in response to both temperature and pressure changes. At the start of each model, we assume that any chloride anomaly due to the formation of the hydrate that is already present or due to hydrate dissociation before the start of the model run has diffused away. We present results showing the transient behavior of the hydrate layer that dissociates into methane and freshwater. The MeBo drilling experiment detected a freshwater anomaly, but it did not directly recover hydrate, i.e., we do not have direct constraints on hydrate saturation values. We varied the initial hydrate saturations with the aim to identify the critical hydrate saturation for which hydrates completely dissociated, and the final chloride values mimicked the observed values (Wallmann et al., 2018).

4.1. Response to BWT_{TF} variations and UiT RSL change (Scenario 1)

The evolution of the hydrate layer in response to the BWT_{TF} time series and a fall in RSL (UiT), which is considered Scenario 1 (Figures 3a and 3c), is illustrated in Figure 4. The model forcing incorporated in this scenario is similar to Wallmann et al. (2018). Table S3 shows the differences between our model and the depressurization model proposed by Wallmann et al. (2018).

We initialized the model at 8.6 ka when the seabed temperature was at 2.05° C, and high sea level favored a thicker initial hydrate column (Figure 4a and Supplementary Figure 1a) compared to Wallmann et al. (2018). We assumed 12% initial hydrate saturation and a gas layer beneath it with 2–4% saturation (Figure 4a), 560 mM Cl^- concentration (Figure 4b) equivalent to pore water salinity of 3.5 wt%, and a steady geothermal gradient of 50° C/km (Figure 4c) in the sediment column. For this scenario, the dissociation of 12% hydrate resulted in the chloride anomaly that best matched the observations (Figures 4a–c).

During 8.6–7.6 ka, the seabed temperature increased from 2 to 2.6 °C, and RSL increased by ~2 m (Figures 3a and 3c). During this time, a small amount of hydrate dissociated at the base of the hydrate stability zone (Figure 4a). Subsequently, RSL dropped by ~3 m, and BWT increased from 2.6 to 3 °C over 7.6–5.9 ka. During this time, hydrate dissociation was governed by warming and depressurization (Figure 4a), freshening the pore water and resulting in a chloride anomaly (Figure 4b). The methane released due to hydrate dissociation flowed upward through the stability zone and vented into the ocean. When the BWT reduced to 2.5° C, such as around 5.3 ka, methane was converted into hydrate and chloride concentration increased at shallower depths (Figures 4a and 4b). In the Wallmann et al. (2018) model, shallow hydrate reformation was not considered, and methane vented rapidly. From 5 ka to 0.4 ka, RSL fall continued to erode the hydrate layer. Between 0.4–0.08 ka, the remaining hydrate layer dissociated due to high BWT conditions (>2.5 °C), since the RSL change was negligible, and the geothermal gradient shifted toward the steady geotherm (Figure 4c).

According to the UiT model, isostatic rebound resulted in an ~8 m fall in RSL between 6 ka and present at our study site (Wallmann et al., 2018). Similar to Wallmann et al. (2018), the consequent drop in hydrostatic pressure was responsible for hydrate dissociation. Hydrate saturation in our model is significantly less than their model; however, the initial hydrate layer is six times thicker than their assumption. In the Wallmann et al. (2018) model, the hydrate layer completely dissociated 1000 years BP producing a large chloride anomaly that progressively diffused away, and methane flow ceased. However, in our case, hydrate dissociation was not completed until 80 years BP, at which point it resulted in a chloride minimum in the system. Subsequently, the chloride anomaly diffused away to match the observed values (Figure 4b) and methane flow was maintained at a low rate (Figure 4d).

We also tested an initial hydrate saturation of 10% for this particular pressure-temperature scenario. This model could not fit the observed chloride saturation profile since the hydrate dissociated earlier (Supplementary Figure 3).

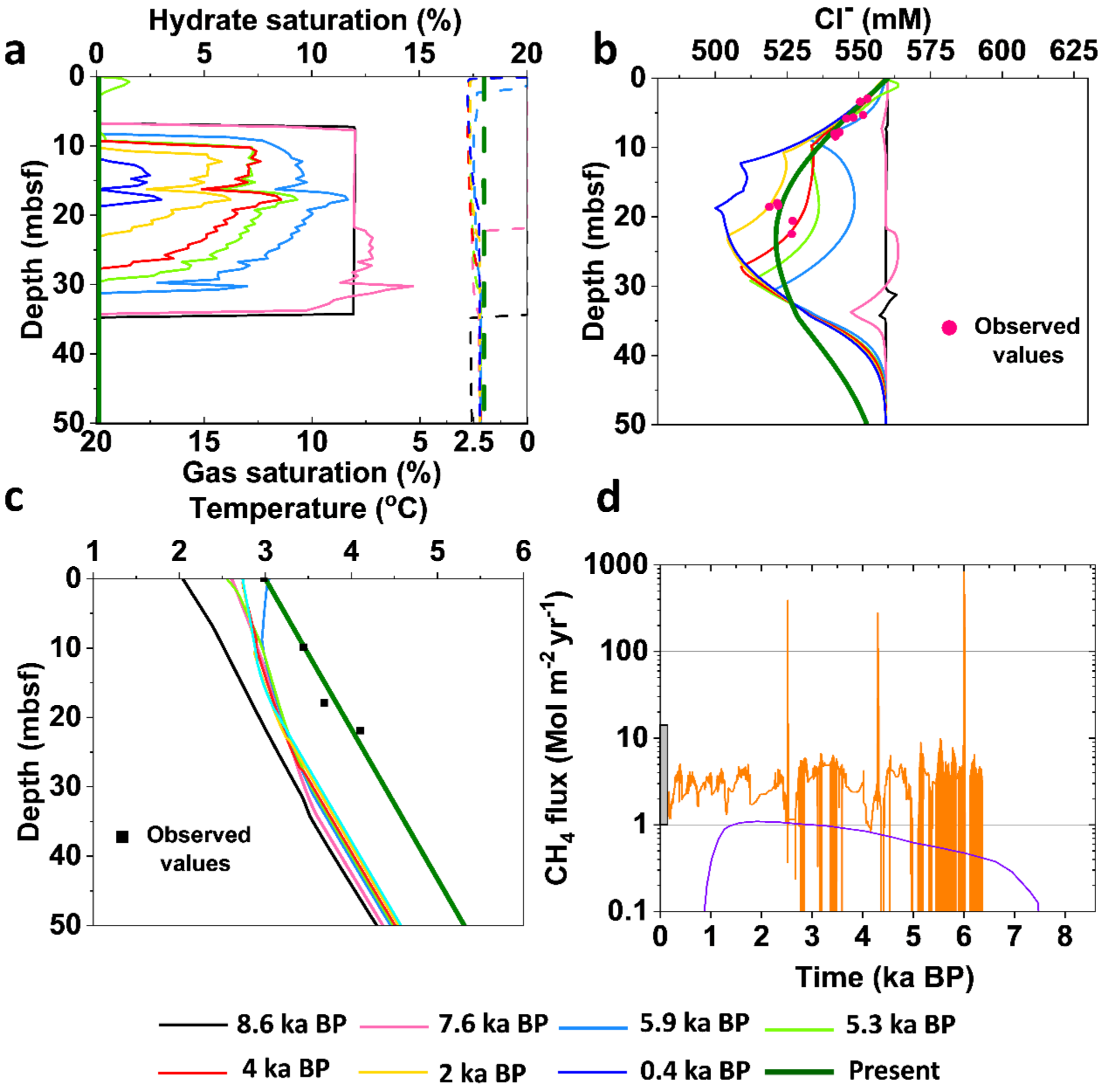

Figure 4. Simulation results for pressure-temperature driven (UiT RSL and BWT_{TF} as model forcing) methane hydrate dissociation. The results are plotted at a series of specific times. (a) Evolution of the hydrate layer thickness and saturation (solid line) and gas layer beneath it (dash line) over the simulation period. Hydrate completely dissociated 80 years BP. (b) Chloride depletion suggests pore water freshening as hydrates dissociate. The chloride concentration started to diffuse away after hydrate dissociation was complete. Pink dots indicate values in cores retrieved at 391 m water depth (Wallmann et al., 2018). (c) Temperature profile in the sediment column. Black squares indicate temperatures measured in drill holes at 391 m water depth. (d) Methane emission rate from sediments into the overlying water column. Modeled fluxes induced by hydrate dissociation over the past 8610 years (orange curve) are compared to the area-averaged range of present-day methane gas fluxes measured at active seeps (grey vertical bar) in the study area (Sahling et al., 2014; Wallmann et al., 2018; Ferré et al., 2020) and methane flux (purple curve) from the depressurization-induced hydrate dissociation model of Wallmann et al. (2018).

4.2. Response to BWT_{TF} variations and ICE-6G_C RSL change (Scenario 2)

In an alternate scenario 2, we tested the impact of BWT_{TF} and ICE-6G_C RSL on the hydrate layer. The ICE-6G_C model predicts RSL rise over the past ~8000 years at the upper continental slope off west Svalbard. The rise in BWT during this period could destabilize hydrate while the RSL rise will have a stabilizing effect; the combined effect of these contrasting factors has not previously been considered.

In this case, we initialized the model at 11.138 ka (rather than 8.6 ka). Initialization at 8.6 ka resulted in a very shallow hydrate layer (0.7–1.2 m) due to the low hydrostatic pressure (~380 m water depth), and the dissociation of this hydrate over 8.6–0.04 ka resulted in a chloride anomaly at relatively shallow depths, whereas the observed chloride anomaly is deeper (10–20 mbsf).

The colder BWT at 11.138 ka favoured a deeper initial hydrate layer (7–22 mbsf). We used an initial hydrate saturation of 60% because this resulted in the chloride anomaly that best matched the observations (Figure 5a). During the initial 1100 years of the simulation, intermittent bottom water warming led to enhanced hydrate dissociation with substantial methane and freshwater release (Figures 5a–c and Supplementary Figure 4). At ~10 ka, hydrate saturation was reduced to 40%. Over the period 10–8 ka, there was a slight RSL fall, resulting in a hydrostatic pressure decrease, and this was accompanied by bottom water cooling (2.7–2 °C, Figures 3a, and 3c). Dissociation slowed due to the bottom water cooling, but the sediment column remained outside the hydrate stability. Since 4 ka, the rise in RSL is predicted to have been small (Figure 3c). The remaining hydrate layer completely dissociated at 40 years BP due to warm bottom water conditions (>2.5 °C). The resulting chloride anomaly started to diffuse away, and the final chloride values are consistent with the observations (Figure 5b). The methane flow (Figure 5d) is predicted to have been highest during the earliest Holocene (11.2–10 ka), continuing through to the present day at a reduced rate. In this scenario, the BWT rise was primarily responsible for hydrate destabilization despite the RSL rise.

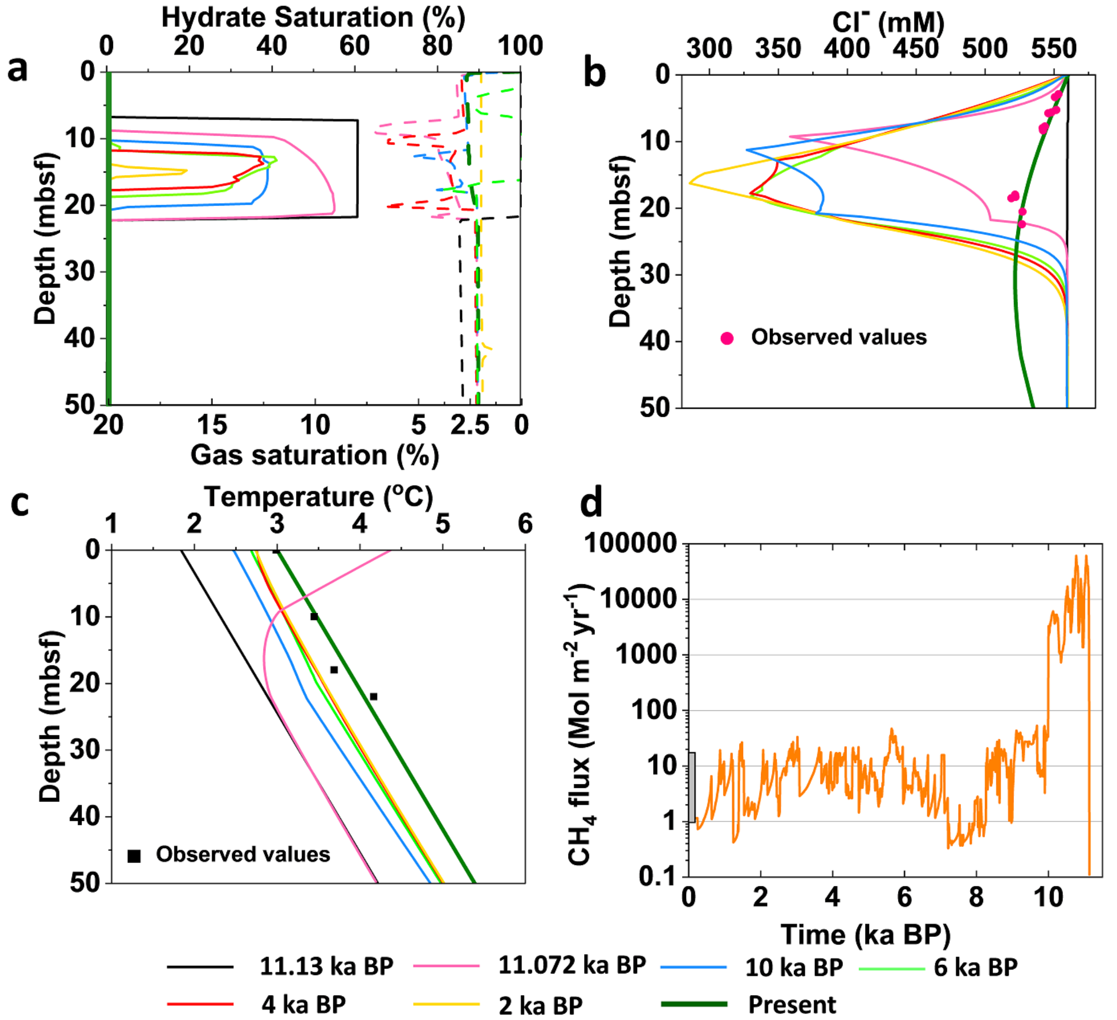

Figure 5. Simulation results for pressure-temperature driven hydrate dissociation forced by ICE-6G_C RSL and BWT_{TF} over the past 11000 years. (a) Evolution of the hydrate layer thickness and saturation over the simulation period. Solid lines mark hydrate saturation and dashed lines mark gas saturation. Hydrate completely dissociated 40 years BP. (b) Dissolved chloride concentration. (c) Temperature profile in the sediment column. Black squares indicate temperatures measured in drill holes at 391 m water depth. The steep rise in temperature towards the seafloor at 11.072 ka reflects the sharp increase in BWT (Figure 3a) imposed at the top boundary cell. Temperature profiles at selected times are shown for clarity. (d) Modeled methane emission rates from sediments into the overlying ocean are compared to the area-averaged range of present-day methane gas fluxes measured at active seeps (grey vertical bar) in the study area (Sahling et al., 2014; Wallmann et al., 2018; Ferré et al., 2020). The methane flow rate was highest during the early Holocene.

4.3. Response to BWT_C variations with UiT and ICE-6G_C RSL change (Scenarios 3 and 4)

In two additional scenarios, we applied BWT_C with UiT RSL (Scenario 3) and BWT_C with ICE-6G_C RSL (Scenario 4) to the hydrate layer. To investigate the development of hydrate in each of these cases, we initialized the model when the BWT_C attained a minimum value of 1.4 °C at 3.16 ka (Figure 3b) using a hydrate saturation of 5% and we ran the model to observe changes in the hydrate layer. Simulation results for scenarios 3 and 4 are shown in Figures 6a-d and 6e-h, respectively.

In scenario 3 (BWT_C+UiT RSL), hydrate dissociation was triggered by depressurization and BWT rise, while in scenario 4 (BWTc+ICE-6G_C RSL), dissociation was exclusively induced by bottom water warming. Initially, gas flowed through the hydrate stability zone (Figures 6a and 6e) and was converted into hydrates, increasing hydrate saturation by ~10–15% as well as chloride concentration (Figures 6b and 6f). The BWT_C record documents two prominent warming pulses (BWT>2.5 °C) at ~1.5 ka and ~0.7 ka (Figure 3b). During these warming episodes, the shallowest hydrate dissociated in both models, and gas reached the seafloor. Hydrate completely dissociated at 53 and 49 years BP in scenarios 3 and 4, respectively, and the final chloride anomalies matched the observed values at the end of the simulations (Figures 6b and 6f). The temperature profiles migrated toward the steady geotherm once the hydrate was exhausted (Figures 6c and 6g). Chloride sensitivity was gauged by varying the initial hydrate saturation. The final chloride values for the model with hydrate saturation more than 5% did not fit the observed chloride profile.

We also compared the response of the hydrate layer to the BWT reconstruction of Marín-Moreno et al. (2013) (refer to section 3.2). In this case, we initialized the model with 5% hydrate saturation (Supplementary Figures 5a and 5d) at 2.16 ka and forced it using BWT_M (Figure 3b) and both sets of RSL values (UiT and ICE-6G_C) (Figure 3c). In these cases, hydrate dissociated completely at 49 and 46 years BP for BWT_M+ UiT RSL and BWT_M+ ICE-6G_C RSL, respectively, and final chloride values matched the present-day observations (Supplementary Figure 5). Although there are differences between BWT_C and BWT_M over the past 2 ka, model outputs at the end of the simulations did not show any major differences.

The experiments described above were initialized in the late Holocene. To check whether some hydrates could have survived warming episodes earlier in the Holocene, we initialized the model with a high hydrate saturation of 60%, as used in Wallmann et al. (2018), at 11.2 ka (Supplementary Figures 6 and 7). In the BWT_C and ICE-6G_C scenario, hydrate dissociation was completed at 10.6 ka (Supplementary Figure 6a) and was driven by seabed warming and minor RSL fall (~2 m). In the BWT_C and UiT scenario, the hydrate layer completely dissociated at 9.6 ka (Supplementary Figure 7a) in response to early Holocene warming despite ~10 m RSL rise. In both cases, the chloride concentration was restored in the next thousand years (Supplementary Figures 6b and 7b). The equivalent early Holocene warming model by Wallmann et al. (2018) also showed complete hydrate dissociation by 10.7 ka; however, they did not consider any RSL change.

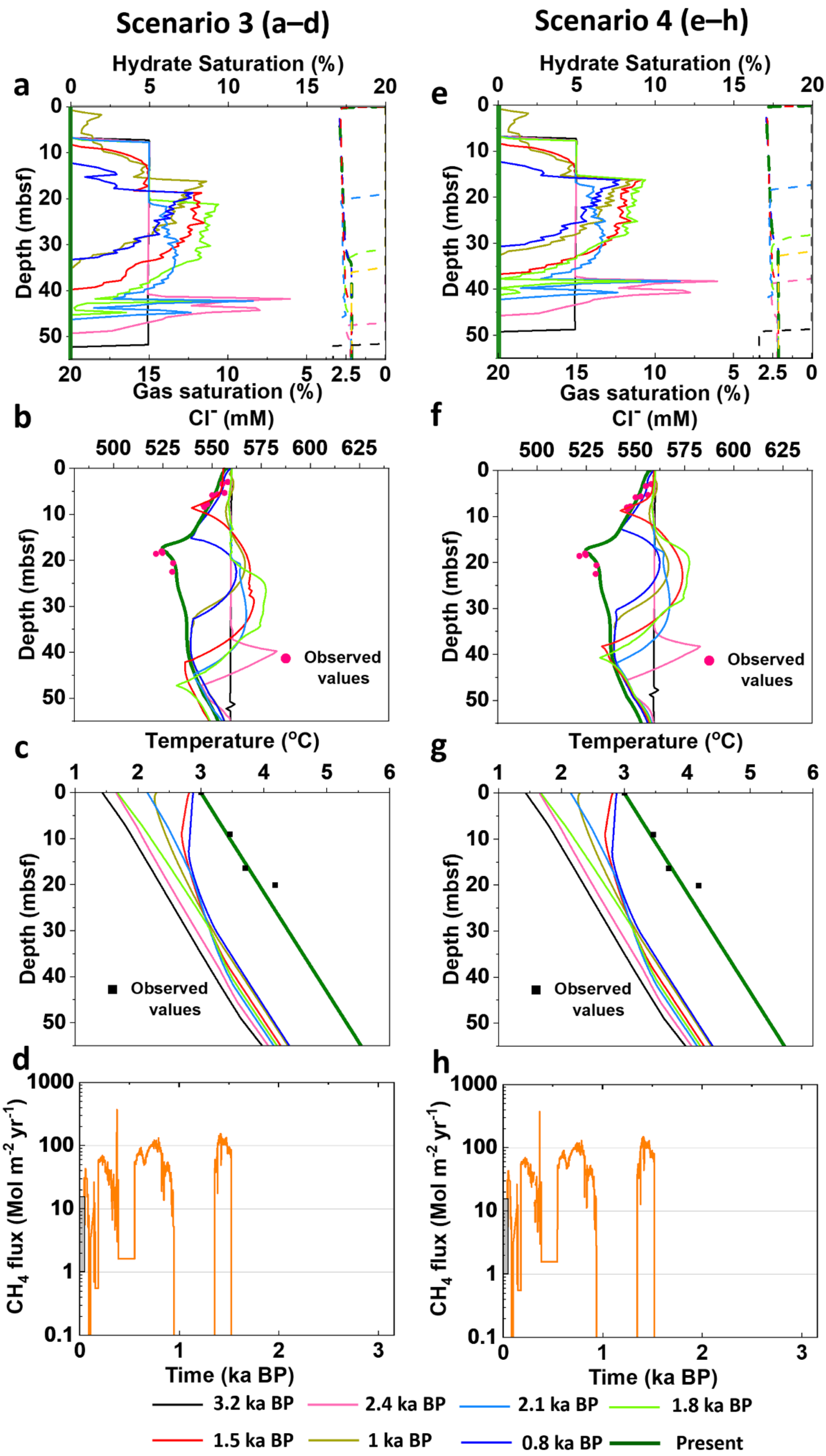

Scenario 3 (a–d)
Scenario 4 (e–h)
a
e
Hydrate Saturation (%)
Gas saturation (%)
Depth (mbsf)
b
f
Cl⁻ (mM)
Observed values
c
g
Temperature (°C)
Observed values
d
h
CH4 flux (Mol m-2 yr-1)
Time (ka BP)
3.2 ka BP
2.4 ka BP
2.1 ka BP
1.8 ka BP
1.5 ka BP
1 ka BP
0.8 ka BP
Present

Figure 6. Simulation results show methane hydrate dissociation forced by BWT_C + UiT RSL (a–d) and BWT_C + ICE-6G_C RSL (e–h) over the past 3160 years (Figures 3b and 3c). (a, e) Evolution of the hydrate layer thickness and saturation over the simulation period. Solid lines mark hydrate saturation and dashed lines mark gas saturation. Hydrate dissociated at the base, and gas migrated through the hydrate stability zone. Hydrate completely dissociated at 53 and 49 years BP in scenarios 3 and 4, respectively. (b, f) Change in dissolved chloride concentration. Hydrate dissociation caused pore water freshening. The chloride concentration started to diffuse after the completion of hydrate dissociation, and the final profiles match the present-day observations (dots). (c, g) The temperature profile in the sediment column. Black squares indicate temperatures measured in drill holes at 391 m water depth. (d, h) Methane emission rate from sediments into the overlying ocean (orange curve) and area-averaged range of present-day methane gas fluxes (grey vertical bar) in the study area (Sahling et al., 2014; Wallmann et al., 2018; Ferré et al., 2020).

4.4. Response to final 38 years of BWT changes

It is evident from the previous long-time series runs that complete hydrate dissociation at this site was possible well before the accelerated bottom water warming during 1978–2008 (Westbrook et al., 2009). For example, dissociation of 12% hydrate was complete at 80 years BP in scenario 1 (BWT_{TF} and UiT RSL, Figure 4a), while in scenarios 3 and 4, covering the past ~3200 years (BWT_C and UiT RSL, Figure 6a and BWT_C and ICE-6G_C RSL, Figure 6e), 5% hydrate completely dissociated around 50 years BP.

In such cases, we examine whether hydrate reformation and subsequent dissociation were possible over the last 38 years in our model runs (1978–2016). Several factors provided suitable conditions for hydrate reformation during this period. During the previous episode of hydrate dissociation, pore water freshening would have enhanced hydrate stability. Similarly, gas from previously dissociated hydrate and deeper sources would have been available to be converted into hydrate during cold BWT conditions. Importantly, any new hydrate formation will have erased any earlier chloride depletion anomaly because chloride is excluded from the hydrate during the reformation.

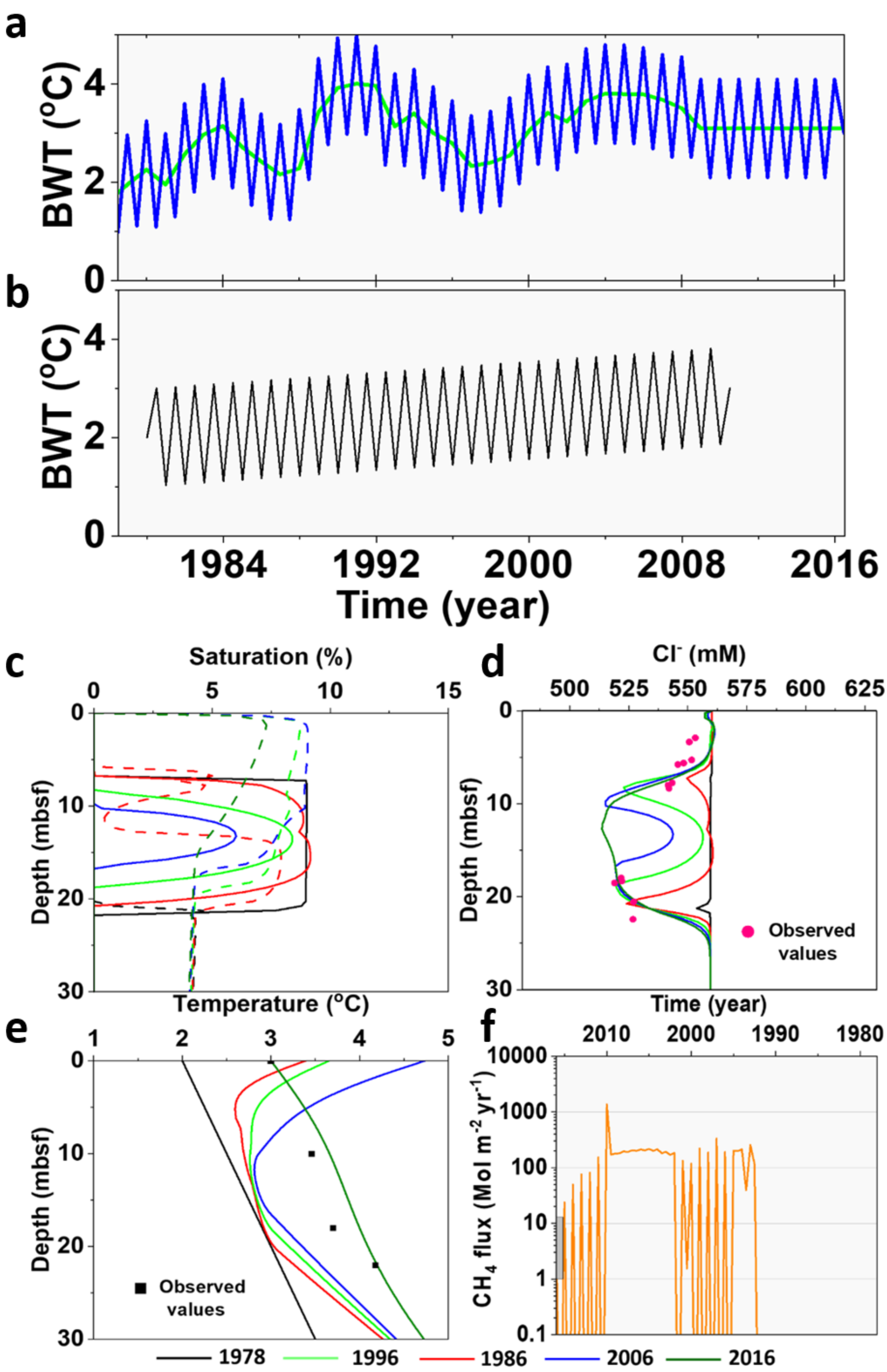

a
BWT (°C)
b
BWT (°C)
1984
1992
2000
2008
2016
Time (year)
c
Saturation (%)
Depth (mbsf)
Temperature (°C)
d
Cl⁻ (mM)
Depth (mbsf)
Observed values
Time (year)
e
Depth (mbsf)
Observed values
f
CH_4 flux (Mol m⁻² yr⁻¹)
1978
1996
1986
2006
2016

510

Figure 7. BWT variations at 400 m water depth off west Svalbard and simulation results showing the behavior of hydrate forced by BWT variations over 1978–2016 in a sediment column with permeability 10^{-13} m^2. (a) The instrumental record of BWT during 1978–2016 (Green curve, Ferré et al. 2012) with seasonal fluctuations of ±1°C (Blue) following Riedel et al. (2018). (b) The 1980–2010 linear temperature rise from 2–3°C was adopted by Wallmann et al. (2018) with seasonal fluctuations of ±1°C. (c) Methane hydrate saturation over the simulation period. The initial hydrate saturation was 9% in 1978. Solid lines mark hydrate saturation and dashed lines mark gas saturation. Hydrate saturation decreased with progressive thermal dissociation. Hydrate completely dissociated 2 years before the end of the model run. (d) Dissolved chloride concentration. The final chloride profile provides a good fit to the observations. (e) The temperature profile in the sediment column. Black squares indicate temperatures measured in drill holes at 391 m water depth. (f) Modeled methane fluxes induced by methane hydrate dissociation compared to the area-averaged range of present-day methane gas fluxes measured at active seep sites (grey vertical bar) (Ferré et al., 2020). In the experiment, methane appeared at the seabed 14 years after the onset of warming.

Our 38-year run (1978–2016), driven by the BWT time series shown in Figure 7a, finds that an initial hydrate layer with 9% hydrate saturation completely dissociates and produces a chloride profile that matches the observations (Figures 7c and 7d). Since the RSL change in past 4 decades is negligibly small, we did not include RSL change in this model. The net 1°C BWT (Figures 7a and 7e) rise led to hydrate dissociation, and the resulting methane flowed through the hydrate stability zone (Figure 7c). Methane appeared at the seabed 14 years after the onset of warming when we considered a permeability of 10^{-13} m^2 (Figure 7f). We observed periodicity in methane flow (Figure 7f) that is attributed to seasonally-induced hydrate formation and dissociation at a shallow depth. The seasonal fluctuations in BWT (Figure 7a) strongly affected the top 10 m of the sediment column, where we find repeated episodes of shallow hydrate reformation and dissociation during colder and warmer conditions, respectively.

Previously, Wallmann et al. (2018) ran a 30-year model (1980–2010) driven by a linear temperature increase from 2 to 3 °C that included seasonal temperature variations ±1°C (Figure 7b). The initial hydrate layer in their model was at 10–30 mbsf, and hydrate saturation was varied in the range of 6–8%. Hydrate did not completely dissociate by the end of their model run, and the chloride anomaly could not be reproduced. Hence, they concluded that the thermal dissociation of hydrates over the past three decades was unlikely. Significant time and energy are required to dissociate 6–8 % hydrate. Although measured down-core temperature gradients lie in 45–50 °C/km (Riedel et al., 2018), their 30-year model assumed a geothermal gradient of 45 °C/km.

Our model was run for an additional 8 years compared to Wallmann et al. (2018), so there was sufficient time for hydrate dissociation. The heat flux ($10x10^{-2}$ W m^{-2}) applied at the base of our model resulted in a geothermal gradient of 50° C/km in the sediment column, which, in turn, resulted in a thinner initial hydrate layer (14 m thick, 7–21 mbsf) than the 20 m thickness considered by Wallmann et al. (2018). Our thinner hydrate layer completely dissociated over 38 years. However, when we considered a lower geothermal gradient (45° C/km) by applying a heat flux of $9x10^{-2}$ W m^{-2}, the initial hydrate layer was thicker (22 m thick, 7–29 mbsf). It did not completely dissociate after 38 years.

We also tested lower (10^{-15} m^2) and higher permeability (10^{-11} m^2) scenarios (Supplementary Figure 8) and different irreducible gas saturation (S_{irg}) values ranging between 2–10% (Ma et al., 2020). We found that hydrate dissociated completely in all cases, and the methane flow rate was very sensitive to the permeability and S_{irg} values (Thatcher et al., 2013). As expected, a reduction in permeability caused a delay in the arrival of the methane at the seabed (Supplementary Figure 9a), while an increase in the S_{irg} value caused a delay in the arrival of the methane at the seabed and a decline in the maximum methane flux (Supplementary Figure 9b).

The simulations described in this section emphasize the role of recent BWT rise as a potential cause for hydrate dissociation and pore water freshening. They also illustrate the role of interannual temperature changes in controlling changes in seafloor methane flux in response to near seafloor hydrate dissociation-formation stages.

5. Discussion

We have examined the impact of RSL change coupled with BWT variations on hydrate west of Svalbard at 391 m water depth, where recent drilling confirmed pore water freshening due to hydrate dissociation. Table 1 summarizes model outputs from scenarios where the final chloride anomaly and subsurface temperature profile closely match the present-day observations.

The previous modelling by various authors either emphasized the role of temperature rise or RSL fall in explaining hydrate destabilization. For example, Thatcher et al. (2013), Marín-Moreno et al. (2013), and Marín-Moreno et al. (2015) considered the effects of BWT on hydrates, while Wallmann et al. (2018) attributed hydrate dissociation to RSL fall at constant BWT. Extending these studies, we have examined the fate of hydrates in response to the combined effects of a plausible set of BWT and RSL values.

We have demonstrated plausible scenarios of hydrate dissociation based on RSL reconstruction and BWT changes that show prominent millennial to seasonal changes over the past 8000 years at different time scales (decadal to seasonal). All of the scenarios considered here predict thinning of the hydrate layer from the base during the Holocene, releasing methane that can get trapped in shallow sediments under cold BWT conditions (<2.5° C). Sharp rises in BWT dissociate the shallow hydrates and enhance gas flow at the seabed. Periods of high methane flow at the seabed could lead to seep-carbonate accumulation at the feather edge of hydrate stability. The precipitated carbonate can influence benthic ecosystems since it provides hardground shelter for them (Wilson et al., 2007). Thicker carbonate accumulations of varying ages could be related to multiple episodes of hydrate dissociation (Berndt et al., 2014). Our modelling shows a range of possible past methane emission scenarios. Future work should focus on mineralogical and isotopic studies of authigenic carbonates (e.g., Liang et al., 2017) to unravel fluid sources, long-term seepage dynamics, and the fate of Arctic methane hydrates.

Our results based on coupled BWT_{TF} and UiT RSL values (Scenario 1) challenge the hypothesis that a fall in RSL was the sole cause of hydrate dissociation over 8–1 ka (Wallmann et al., 2018). The depressurization model proposed by Wallmann et al. (2018) only considered a constant BWT over 8–0.1 ka. By using the UiT RSL in combination with the more realistic BWT_{TF} curve, we find that pulses of warm bottom water temperatures (>2.5° C) also contributed to hydrate dissociation together with depressurization. The initial hydrate saturation was significantly higher (60%) in the Wallmann et al. (2018) model compared to the initial saturation (12%) in our BWT_{TF} and UiT RSL scenario. Previously inferred hydrate saturations in the top 50 m of glaciomarine sediments on the upper continental slope of Svalbard, in water depths of 480–866 m, range between 5–22% (Chabert et al., 2011 and Goswami et al., 2016). While the initial hydrate saturations considered here are within this range in most cases, we infer a higher value (60%) in the model forced by BWT_{TF} and ICE-6G_C RSL (Scenario 2). We needed such a high initial hydrate saturation to generate the chloride anomaly that mimics present-day observations. In scenario 2, hydrates of such high saturation slowly dissociated over a prolonged period (11138 years). The model shows a prolonged record of methane emission at the seabed, with methane flux progressively decreasing with time (Figure 5d).

Based on their model (UiT RSL), Wallmann et al. (2018) concluded that methane fluxes from hydrate dissociation ceased at 1 ka upon completion of depressurization-induced dissociation, and the present-day gas seeps are not related to warming-induced hydrate dissociation. This inference disagrees with the findings of Veloso-Alarcon et al. (2019) and Ferré et al. (2020), who proposed that the present-day methane flux is likely controlled by temperature-driven seasonal hydrate dynamics. In our simulation using the BWT_{TF} and UiT RSL, complete hydrate dissociation takes longer than in Wallmann et al. (2018) mainly because some time is required between the onset of hydrate dissociation and methane reaching the seabed and it depends on effective permeability, porosity, irreducible gas saturation, hydrate saturation, distance between the top of the hydrate layer and the seafloor (Thatcher et al., 2013). For this scenario, the modeled methane flux at present (year 2016) lies at the lower end of the range of observed values (1 mol m^{-2} $year^{-1}$, compared with 1–13 mol m^{-2} $year^{-1}$, Ferré et al., 2020), suggesting that other possible explanations for the methane seeps should be investigated.

Despite the possibility of several episodes of hydrate formation and dissociation in the past, the latest episode of hydrate formation and subsequent warming (1978–2016) stands out as a strong possibility that can explain the observed pore water freshening and variations in methane flux at the seabed. The observed gas flare activity shows large variations that are strongly influenced by seasonal hydrate dynamics (Berndt et al., 2014; Veloso-Alarcon et al., 2019; Ferré et al., 2020). This pattern is well explained by our 38-year simulation (1978–2016), where the initial 9% hydrate saturation completely dissociated, and hydrate dynamics are clearly influenced by decadal- and seasonal-scale BWT fluctuations (Figure 7f). There is seismic evidence of gas (Chabert et al., 2011; Sarkar et al., 2012) in the top 100 m of the sediment column at the upper continental slope (water depths 350–1200 m). In all the cases we considered (Table 1), our modeling predicts that hydrates have completely dissociated prior to 1978. However, the combination of the delayed upwards migration of the resulting methane through vertical fractures and permeable strata (Sarkar et al., 2012) and colder BWTs, such as the remarkable cooling (10-year) during the late 1970s (Westbrook et al., 2009), likely created favourable conditions for hydrate re-formation. Since no hydrates were recovered by the drilling, ocean bottom warming must have completely dissociated these newly-formed hydrates to explain the observed pore-water freshening. Therefore, there is insufficient evidence to reject the (*recent*) warming-induced hydrate dissociation hypothesis (Westbrook et al., 2009) in explaining the present-day methane seeps off west Svalbard.

Our 38-year model provides valuable insights into the response of methane hydrates to recent warming at the feather edge of hydrate stability in this area. Moreover, it evidences the importance of reducing uncertainty in the predictions of methane emissions, particularly on the continental shelf. Since the shelf regions are at shallower water depths (100–200 m), seafloor methane emissions have a greater chance to reach the atmosphere. Even if methane does not reach the atmosphere in these areas, methane dissolution and its oxidation in the ocean can cause local changes in pH, thereby affecting the local marine biodiversity

(Valentine et al., 2001; Riebesell, 2008). Although gas emission activity could substantially subside at the feather edge of hydrate stability during bottom water cooling on the upper continental slope (~390 m), deeper gas can still be deflected by the impermeable hydrate layer and migrate upslope towards the shelf through permeable beds (Sarkar et al., 2012; Veloso-Alarcon et al., 2019). The beds outcrop at the shelf, and methane is released directly into the ocean. Veloso-Alarcon et al. (2019) reported enhanced methane flux on the continental shelf (100–200 m water depths) compared to the upper slope during cooler BWT conditions since the shelf is outside the gas hydrate stability. Strong methane emission has a greater chance of reaching the sea surface and atmosphere, contributing to further warming (Westbrook et al., 2009).

Model forcing and duration of simulation (2016 represents 'Present')	Time taken to completely dissociate hydrate (years)	Initial hydrate saturation, initial hydrate layer thickness	Correlation between observed chloride anomaly and final chloride values obtained from the model	Methane flux at the end of the simulation (Observed area-averaged methane flux is 1–13 Mol m^{-2} y^{-1})
Scenario 1: BWT_{TF} + UiT RSL (8.6–0 ka)	8520	12%, 30 m	0.9	1
Scenario 2: BWT_{TF} + ICE-6G_C RSL (11.138–0 ka)	11098	60%, 15 m	0.8	1
Scenario 3: BWT_{C} + UiT RSL (3.16–0 ka)	3107	5%, 45 m	0.9	2.25
Scenario 4: BWT_{C} + ICE-6G_C RSL (3.16–0 ka)	3111	5%, 42 m	0.9	2.2
Scenario 5: BWT from (1978–2016) (Ferré et al., 2012)	36	9%, 14 m	0.94	7

Table 1. Summary table showing the modeling scenarios and quantification of how well the final results (chloride values, and methane flux) matched the observations.

6. Conclusions

We have re-examined the fate of Arctic marine hydrates in response to BWT and RSL changes at the landward limit of hydrate stability off west Svalbard. We have considered an alternative ice history model (ICE-6G_C) that suggests RSL rise and contradicts the RSL fall predicted by the UiT model over the past 8000 years used in a previous modelling study in the area (Wallmann et al., 2018). We demonstrate that with the available constraints, multiple episodes of hydrate formation and dissociation are still possible based on a comprehensive scenario testing approach that has never been attempted before for such a long-time scale.

In the simulation that used the UiT scenario, we found that although RSL fall may have triggered hydrate dissociation, decadal-scale BWT fluctuations (BWT_{TF} and BWT_{C}) played a critical role in controlling hydrate dynamics. Specifically, in these scenarios the eventual fate of methane released from depressurization-induced hydrate dissociation depended on BWT. Warmer seabed temperatures (e.g., >2.5°C) prevented the shallow hydrate reformation, allowing gas to flow through the hydrate stability zone and into the ocean. On the other hand, colder bottom water temperatures facilitated shallow hydrate reformation. In the simulations that used the ICE-6G_C scenario, hydrate dissociation was primarily caused by warming of bottom waters, which overrode the stabilising effect of RSL rise.

We have not been able to determine the actual RSL and BWT scenario through which the hydrate system evolved since several scenarios produce outputs that match the present-day observations. However, we demonstrate that earlier hydrates completely dissociated before the late 1970s' bottom water cooling episode, irrespective of the assumed scenario. During this cooling episode, hydrate could have reformed and then dissociated in response to BWT rise over the period 1978–2016. The gas produced by dissociation takes time to migrate to the seabed and can explain the modern methane seeps. Seasonal warming and cooling cycles impact hydrate dynamics and can explain the large observed variations in methane flux. The pore water freshening observed in the marine sediments is indicative of the latest episode of hydrate destabilization caused by the latest episode of seabed warming.

If bottom water warming continues at an accelerated rate, we can expect downslope migration of the landward limit of hydrate stability. The results presented here bring into focus the necessity to closely monitor the effect of warming Atlantic waters on hydrates because continued warming may degrade more Arctic marine hydrates in the impending future at current or enhanced rates.

Acknowledgments

SS was supported by the Science and Engineering Research Board (SERB Act 2008) as a part of its Earth and Atmospheric Science programme Start-up Research Grant (SRG/2019/001072) and SS also thanks DST FIST (Grant number SR/FST/ES-I/2018/25) for infrastructure support. We thank Henry Patton for providing information about the UiT Ice sheet modelling. We thank the Associate Editor, one anonymous reviewer, and Peter Flemings for their detailed and helpful comments.

Open research

The bathymetric image shown in Figure 1 was derived from the Norwegian Hydrographic Service (NHS) data and the bathymetric data acquired during the JR211 cruise. The JR211 bathymetric data can be obtained from www.bodc.ac.uk by contacting enquiries@bodc.ac.uk. The NHS bathymetric data can be accessed from https://dybdedata.kartverket.no/DybdedataInnsyn/. The hydrate model results were generated using Tough+Hydrate v1.5, which can be obtained from https://tough.lbl.gov/licensing-download/tough-licensing-download/.

References

Argus, D. F., Peltier, W. R., Drummond, R., & Moore, A. W. (2014). The Antarctica component of postglacial rebound model ICE-6G_C (VM5a) based on GPS positioning, exposure age dating of ice thicknesses, and relative sea level histories. *Geophysical Journal International*, *198*(1). https://doi.org/10.1093/gji/ggu140

Auriac, A., Whitehouse, P. L., Bentley, M. J., Patton, H., Lloyd, J. M., & Hubbard, A. (2016). Glacial isostatic adjustment associated with the Barents Sea ice sheet: A modelling inter-comparison. *Quaternary Science Reviews*, *147*, 122–135. https://doi.org/10.1016/J.QUASCIREV.2016.02.011

Berndt, C., Feseker, T., Treude, T., Krastel, S., Liebetrau, V., Niemann, H., et al. (2014). Temporal Constraints on Hydrate-Controlled Methane Seepage off Svalbard. *Science*, *343*(6168), 284–287. https://doi.org/10.1126/science.1246298

Boetius, A., & Wenzhöfer, F. (2013). Seafloor oxygen consumption fuelled by methane from cold seeps. *Nature Geoscience*, *6*(9). https://doi.org/10.1038/ngeo1926

Borowski, W. S., Paull, C. K., & Ussler, W. (1996). Marine pore-water sulfate profiles indicate in situ methane flux from underlying gas hydrate. *Geology*, *24*(7). https://doi.org/10.1130/0091-7613(1996)024<0655:MPWSPI>2.3.CO;2

Chabert, A., Minshull, T. A., Westbrook, G. K., Berndt, C., Thatcher, K. E., & Sarkar, S. (2011). Characterization of a stratigraphically constrained gas hydrate system along the western continental margin of Svalbard from ocean bottom seismometer data. *Journal of Geophysical Research*, *116*(B12). https://doi.org/10.1029/2011JB008211

Comiso, J. C., Parkinson, C. L., Gersten, R., & Stock, L. (2008). Accelerated decline in the Arctic sea ice cover. *Geophysical Research Letters*, *35*(1). https://doi.org/10.1029/2007GL031972

Dickens, G. R. (2003). Rethinking the global carbon cycle with a large, dynamic and microbially mediated gas hydrate capacitor. *Earth and Planetary Science Letters*, *213*(3–4). https://doi.org/10.1016/S0012-821X(03)00325-X

Dumke, I., Burwicz, E. B., Berndt, C., Klaeschen, D., Feseker, T., Geissler, W. H., & Sarkar, S. (2016). Gas hydrate distribution and hydrocarbon maturation north of the Knipovich Ridge, western Svalbard margin. *Journal of Geophysical Research: Solid Earth*, *121*(3). https://doi.org/10.1002/2015JB012083

Ferré, B., Mienert, J., & Feseker, T. (2012). Ocean temperature variability for the past 60 years on the Norwegian-Svalbard margin influences gas hydrate stability on human time scales. *Journal of Geophysical Research: Oceans*, *117*(C10). https://doi.org/10.1029/2012JC008300

Ferré, B., Jansson, P. G., Moser, M., Serov, P., Portnov, A., Graves, C. A., et al. (2020). Reduced methane seepage from Arctic sediments during cold bottom-water conditions. *Nature Geoscience*, *13*(2). https://doi.org/10.1038/s41561-019-0515-3

Forman, S. (2004). A review of postglacial emergence on Svalbard, Franz Josef Land and Novaya Zemlya, northern Eurasia. *Quaternary Science Reviews*, *23*(11–13). https://doi.org/10.1016/j.quascirev.2003.12.007

Goswami, B. K., Weitemeyer, K. A., Minshull, T. A., Sinha, M. C., Westbrook, G. K., & Marín-Moreno, H. (2016). Resistivity image beneath an area of active methane seeps in the west Svalbard continental slope. *Geophysical Journal International*, *207*(2). https://doi.org/10.1093/gji/ggw330

Haacke, R. R., & Westbrook, G. K. (2006). A fast, robust method for detecting and characterizing azimuthal anisotropy with marine *PS* converted waves, and its application to the west Svalbard continental slope. *Geophysical Journal International*, *167*(3). https://doi.org/10.1111/j.1365-246X.2006.03186.x

Haacke, R. Ross, Westbrook, G. K., & Peacock, S. (2009). Layer stripping of shear-wave splitting in marine *PS* waves. *Geophysical Journal International*, *176*(3). https://doi.org/10.1111/j.1365-246X.2008.04060.x

Hassol Arctic Climate Impact Assessment. Arctic Monitoring and Assessment Programme. Program for the Conservation of Arctic Flora and Fauna. International Arctic Science Committee., S. (2004). *Impacts of a warming Arctic: Arctic Climate Impact Assessment*. Cambridge, U.K.; New York, N.Y.: Cambridge University Press.

Jakobsson, M., Mayer, L. A., Bringensparr, C., Castro, C. F., Mohammad, R., Johnson, P., et al. (2020). The International Bathymetric Chart of the Arctic Ocean Version 4.0. *Scientific Data*, *7*(1). https://doi.org/10.1038/s41597-020-0520-9

Holliday, N. P., Hughes, S. L., Bacon, S., Beszczynska-Möller, A., Hansen, B., Lavín, A., et al. (2008). Reversal of the 1960s to 1990s freshening trend in the northeast North Atlantic and Nordic Seas. *Geophysical Research Letters*, *35*(3). https://doi.org/10.1029/2007GL032675

James, R.H., Connelly, D., Graves, C., Alker, B., Cole, C., Wright, I., Kolomijeca, A. and Party Jr, S.S., 2011, December. Fate of methane released from Arctic shelf and slope sediments and implications for climate change. In *AGU Fall Meeting Abstracts* (Vol. 2011, pp. GC52A-07).

Kennett, J. P., Cannariato, K. G., Hendy, I. L., & Behl, R. J. (2003). *Methane Hydrates in Quaternary Climate Change: The Clathrate Gun Hypothesis*. Washington, D. C.: American Geophysical Union. https://doi.org/10.1029/054SP

Knies, J., Matthiessen, J., Vogt, C., Laberg, J. S., Hjelstuen, B. O., Smelror, M., et al. (2009). The Plio-Pleistocene glaciation of the Barents Sea–Svalbard region: a new model based on revised chronostratigraphy. *Quaternary Science Reviews*, *28*(9–10). https://doi.org/10.1016/j.quascirev.2008.12.002

Kretschmer, K., Biastoch, A., Rüpke, L., & Burwicz, E. (2015). Modeling the fate of methane hydrates under global warming. *Global Biogeochemical Cycles*, *29*(5). https://doi.org/10.1002/2014GB005011

Landvik, J. Y., Ingólfsson, Ó., Mienert, J., Lehman, S. J., Solheim, A., Elverhøi, A., & Ottesen, D. (2008). Rethinking Late Weichselian ice-sheet dynamics in coastal NW Svalbard. *Boreas*, *34*(1). https://doi.org/10.1111/j.1502-3885.2005.tb01001.x

Liang, Q., Hu, Y., Feng, D., Peckmann, J., Chen, L., Yang, S., et al. (2017). Authigenic carbonates from newly discovered active cold seeps on the northwestern slope of the South China Sea: Constraints on fluid sources, formation environments, and seepage dynamics. *Deep Sea Research Part I: Oceanographic Research Papers, 124.* https://doi.org/10.1016/j.dsr.2017.04.015

Liu, X., & Flemings, P. (2009). Dynamic response of oceanic hydrates to sea level drop. *Geophysical Research Letters*, *36*(17). https://doi.org/10.1029/2009GL039821

Ma, X., Sun, Y., Guo, W., Jia, R., & Li, B. (2020). Effects of Irreducible Fluid Saturation and Gas Entry Pressure on Gas Production from Hydrate-Bearing Clayey Silt Sediments by Depressurization. *Geofluids*, *2020*. https://doi.org/10.1155/2020/9382058

Madec G. (2012), NEMO ocean engine. Note du Pole de modélisation, Tech. Rep., 27, Inst. Pierre-Simon Laplace (IPSL), Paris.

Marín-Moreno, H., Minshull, T. A., Westbrook, G. K., & Sinha, B. (2015). Estimates of future warming-induced methane emissions from hydrate offshore west Svalbard for a range of climate models. *Geochemistry, Geophysics, Geosystems*, *16*(5). https://doi.org/10.1002/2015GC005737

Marín-Moreno, H., Minshull, T. A., Westbrook, G. K., Sinha, B., & Sarkar, S. (2013). The response of methane hydrate beneath the seabed offshore Svalbard to ocean warming during the next three centuries. *Geophysical Research Letters*, *40*(19). https://doi.org/10.1002/grl.50985

Mau, S., Römer, M., Torres, M. E., Bussmann, I., Pape, T., Damm, E., et al. (2017). Widespread methane seepage along the continental margin off Svalbard - from Bjørnøya to Kongsfjorden. *Scientific Reports*, *7*(1). https://doi.org/10.1038/srep42997

Le Meur, E., & Huybrechts, P. (1996). A comparison of different ways of dealing with isostasy: examples from modelling the Antarctic ice sheet during the last glacial cycle. *Annals of Glaciology*, *23*, 309–317. https://doi.org/DOI: 10.3189/S0260305500013586

Minshull, T. A., Marín-Moreno, H., Betlem, P., Bialas, J., Bünz, S., Burwicz, E., et al. (2020). Hydrate occurrence in Europe: A review of available evidence. *Marine and Petroleum Geology*, *111*. https://doi.org/10.1016/j.marpetgeo.2019.08.014

Moridis, G. J. (2003). Numerical Studies of Gas Production from Methane Hydrates. *SPE Journal*, *8*(04). https://doi.org/10.2118/87330-PA

Moridis, G. J., M. B. Kowalsky, and K. Pruess (2014), TOUGH+HYDRATE v1.5 user's manual: A code for the simulation of system behavior in hydrate-bearing geological media, Per. LBNL-0149E, Lawrence Berkeley Natl. Lab., Berkeley, Calif.

Nagornov, O. V., Konovalov, Y. V., & Tchijov, V. (2006). Temperature reconstruction for Arctic glaciers. *Palaeogeography, Palaeoclimatology, Palaeoecology*, *236*(1–2). https://doi.org/10.1016/j.palaeo.2005.11.035

Nisbet, E. G. (1990). The end of the ice age. *Canadian Journal of Earth Sciences*, *27*(1). https://doi.org/10.1139/e90-012

Osterkamp, T. (2005). The recent warming of permafrost in Alaska. *Global and Planetary Change*, *49*(3–4). https://doi.org/10.1016/j.gloplacha.2005.09.001

Panieri, G., C. A. Graves, and R. H. James (2016), Paleo-methane emissions recorded in foraminifera near the landward limit of the gas hydrate stability zone offshore western Svalbard,Geochem. Geophys. Geosyst.,17, 521–537, doi:10.1002/2015GC006153.

Patton, H., Hubbard, A., Andreassen, K., Auriac, A., Whitehouse, P. L., Stroeven, A. P., et al. (2017). Deglaciation of the Eurasian ice sheet complex. *Quaternary Science Reviews*, *169*. https://doi.org/10.1016/j.quascirev.2017.05.019

Peltier, W. R., Argus, D. F., & Drummond, R. (2015). Space geodesy constrains ice age terminal deglaciation: The global ICE-6G_C (VM5a) model. *Journal of Geophysical Research: Solid Earth*, *120*(1). https://doi.org/10.1002/2014JB011176

Piechura, J., & Walczowski, W. (2009). Warming of the West Spitsbergen Current and sea ice north of Svalbard. *OCEANOLOGIA*, *51*(2). https://doi.org/10.5697/oc.51-2.147

Polyakov, I. V., Alekseev, G. V., Timokhov, L. A., Bhatt, U. S., Colony, R. L., Simmons, H. L., et al. (2004). Variability of the Intermediate Atlantic Water of the Arctic Ocean over the Last 100 Years. *Journal of Climate*, *17*(23). https://doi.org/10.1175/JCLI-3224.1

Rasmussen, T. L., Thomsen, E., Skirbekk, K., Ślubowska-Woldengen, M., Klitgaard Kristensen, D., & Koç, N. (2014). Spatial and temporal distribution of Holocene temperature maxima in the northern Nordic seas: interplay of Atlantic-, Arctic- and polar water masses. *Quaternary Science Reviews*, *92*. https://doi.org/10.1016/j.quascirev.2013.10.034

Reagan, M. T., Moridis, G. J., Elliott, S. M., & Maltrud, M. (2011). Contribution of oceanic gas hydrate dissociation to the formation of Arctic Ocean methane plumes. *Journal of Geophysical Research*, *116*(C9). https://doi.org/10.1029/2011JC007189

Riebesell, U., Bellerby, R. G. J., Grossart, H.-P., & Thingstad, F. (2008). Mesocosm CO$_{2}$ perturbation studies: from organism to community level. Biogeosciences, 5(4), 1157–1164. https://doi.org/10.5194/bg-5-1157-2008

Riedel, M., Wallmann, K., Berndt, C., Pape, T., Freudenthal, T., Bergenthal, M., et al. (2018). In Situ Temperature Measurements at the Svalbard Continental Margin: Implications for Gas Hydrate Dynamics. *Geochemistry, Geophysics, Geosystems*, *19*(4). https://doi.org/10.1002/2017GC007288

Sahling, H., Römer, M., Pape, T., Bergès, B., dos Santos Fereirra, C., Boelmann, J., et al. (2014). Gas emissions at the continental margin west of Svalbard: mapping, sampling, and quantification. *Biogeosciences*, *11*(21). https://doi.org/10.5194/bg-11-6029-2014

Sarkar, S., Berndt, C., Chabert, A., Masson, D. G., Minshull, T. A., & Westbrook, G. K. (2011). Switching of a paleo-ice stream in northwest Svalbard. *Quaternary Science Reviews*, *30*(13–14). https://doi.org/10.1016/j.quascirev.2011.03.013

Sarkar, S., Berndt, C., Minshull, T. A., Westbrook, G. K., Klaeschen, D., Masson, D. G., et al. (2012). Seismic evidence for shallow gas-escape features associated with a retreating gas hydrate zone offshore west Svalbard. *Journal of Geophysical Research: Solid Earth*, *117*(B9). https://doi.org/10.1029/2011JB009126

Shipley, T. H., M. H. Houston, R. T. Buffler, F. J. Shaub, K. J. McMillen, J. W. Ladd, and J. L. Worzel (1979). Seismic Evidence for Widespread Possible Gas Hydrate Horizons on Continental Slopes and Rises. *AAPG Bulletin*, *63*. https://doi.org/10.1306/2F91890A-16CE-11D7-8645000102C1865D

Solheim, A., Andersen, E. S., Elverhøi, A., & Fiedler, A. (1996). Late Cenozoic depositional history of the western Svalbard continental shelf, controlled by subsidence and climate. *Global and Planetary Change*, *12*(1–4). https://doi.org/10.1016/0921-8181(95)00016-X

Spielhagen, R. F., Werner, K., Sørensen, S. A., Zamelczyk, K., Kandiano, E., Budeus, G., et al. (2011). Enhanced Modern Heat Transfer to the Arctic by Warm Atlantic Water. *Science*, *331*(6016). https://doi.org/10.1126/science.1197397

Stone, H. L. (1970). Probability Model for Estimating Three-Phase Relative Permeability. *Journal of Petroleum Technology*, *22*(02). https://doi.org/10.2118/2116-PA

Thatcher, K. E., Westbrook, G. K., Sarkar, S., & Minshull, T. A. (2013). Methane release from warming-induced hydrate dissociation in the West Svalbard continental margin: Timing, rates, and geological controls. *Journal of Geophysical Research: Solid Earth*, *118*(1). https://doi.org/10.1029/2012JB009605

Valentine, D. L., Blanton, D. C., Reeburgh, W. S., & Kastner, M. (2001). Water column methane oxidation adjacent to an area of active hydrate dissociation, Eel river Basin. Geochimica et Cosmochimica Acta, 65(16), 2633–2640. https://doi.org/https://doi.org/10.1016/S0016-7037(01)00625-1

Van Genuchten, M. T. (1980). A Closed-form Equation for Predicting the Hydraulic Conductivity of Unsaturated Soils. *Soil Science Society of America Journal*, *44*(5). https://doi.org/10.2136/sssaj1980.03615995004400050002x

Veloso-Alarcón, M. E., Jansson, P., De Batist, M., Minshull, T. A., Westbrook, G. K., Pälike, H., et al. (2019). Variability of Acoustically Evidenced Methane Bubble Emissions Offshore Western Svalbard. *Geophysical Research Letters*, *46*(15). https://doi.org/10.1029/2019GL082750

Vorren, T. O., Laberg, J. S., Blaume, F., Dowdeswell, J. A., Kenyon, N. H., Mienert, J., et al. (1998). The Norwegian–Greenland Sea Continental Margins: Morphology and late Quaternary sedimentary processes and environment. *Quaternary Science Reviews*, *17*(1–3). https://doi.org/10.1016/S0277-3791(97)00072-3

Waelbroeck, C., Labeyrie, L., Michel, E., Duplessy, J. C., McManus, J. F., Lambeck, K., et al. (2002). Sea-level and deep water temperature changes derived from benthic foraminifera isotopic records. *Quaternary Science Reviews*, *21*(1–3). https://doi.org/10.1016/S0277-3791(01)00101-9

Wallmann, K., Riedel, M., Hong, W. L., Patton, H., Hubbard, A., Pape, T., et al. (2018). Gas hydrate dissociation off Svalbard induced by isostatic rebound rather than global warming. *Nature Communications*, *9*(1). https://doi.org/10.1038/s41467-017-02550-9

Walter Anthony, K. M., Anthony, P., Grosse, G., & Chanton, J. (2012). Geologic methane seeps along boundaries of Arctic permafrost thaw and melting glaciers. *Nature Geoscience*, *5*(6), 419–426. https://doi.org/10.1038/ngeo1480

Westbrook, G. K., Thatcher, K. E., Rohling, E. J., Piotrowski, A. M., Pälike, H., Osborne, A. H., et al. (2009). Escape of methane gas from the seabed along the West Spitsbergen continental margin. *Geophysical Research Letters*, *36*(15). https://doi.org/10.1029/2009GL039191.

Wilson, D., Alm, J., Laine, J., Byrne, K. A., Farrell, E. P., & Tuittila, E.-S. (2009). Rewetting of Cutaway Peatlands: Are We Re-Creating Hot Spots of Methane Emissions? Restoration Ecology, 17(6), 796–806. https://doi.org/10.1111/j.1526-100X.2008.00416.x

Xu, T., Y. Ontoy, P. Molling, N. Spycher, M. Parini, and K. Pruess (2004), Reactive transport modeling of injection well scaling and acidizingat Tiwi field, Philippines, Geothermics,33(4), 477–491, doi: 10.1016/j.geothermics.2003.09.012.